

## Evaluation of respiratory motion-corrected cone-beam CT at end expiration in abdominal radiotherapy sites: a prospective study

Russell E. Kincaid Jr.<sup>a\*</sup>, Agung E. Hertanto<sup>a</sup>, Yu-Chi Hu<sup>a</sup>, Abraham J. Wu<sup>b</sup>, Karyn A. Goodman<sup>b†</sup>, Hai D. Pham<sup>a</sup>, Ellen D. Yorke<sup>a</sup>, Qinghui Zhang<sup>a‡</sup>, Qing Chen<sup>a</sup> and Gig S. Mageras<sup>a</sup>

<sup>a</sup>Department of Medical Physics, Memorial Sloan Kettering Cancer Center, New York, NY, USA; <sup>b</sup>Department of Radiation Oncology, Memorial Sloan Kettering Cancer Center, New York, NY, USA

### ABSTRACT

**Background:** Cone beam computed tomography (CBCT) for radiotherapy image guidance suffers from respiratory motion artifacts. This limits soft tissue visualization and localization accuracy, particularly in abdominal sites. We report on a prospective study of respiratory motion-corrected (RMC)-CBCT to evaluate its efficacy in localizing abdominal organs and improving soft tissue visibility at end expiration.

**Material and methods:** In an IRB approved study, 11 patients with gastroesophageal junction (GEJ) cancer and five with pancreatic cancer underwent a respiration-correlated CT (4DCT), a respiration-gated CBCT (G-CBCT) near end expiration and a one-minute free-breathing CBCT scan on a single treatment day. Respiration was recorded with an external monitor. An RMC-CBCT and an uncorrected CBCT (NC-CBCT) were computed from the free-breathing scan, based on a respiratory model of deformations derived from the 4DCT. Localization discrepancy was computed as the 3D displacement of the GEJ region (GEJ patients), or gross tumor volume (GTV) and kidneys (pancreas patients) in the NC-CBCT and RMC-CBCT relative to their positions in the G-CBCT. Similarity of soft-tissue features was measured using a normalized cross correlation (NCC) function.

**Results:** Localization discrepancy from the end-expiration G-CBCT was reduced for RMC-CBCT compared to NC-CBCT in eight of eleven GEJ cases (mean  $\pm$  standard deviation, respectively,  $0.21 \pm 0.11$  and  $0.43 \pm 0.28$  cm), in all five pancreatic GTVs ( $0.26 \pm 0.21$  and  $0.42 \pm 0.29$  cm) and all ten kidneys ( $0.19 \pm 0.13$  and  $0.51 \pm 0.25$  cm). Soft-tissue feature similarity around GEJ was higher with RMC-CBCT in nine of eleven cases (NCC =  $0.48 \pm 0.20$  and  $0.43 \pm 0.21$ ), and eight of ten kidneys ( $0.44 \pm 0.16$  and  $0.40 \pm 0.17$ ).

**Conclusions:** In a prospective study of motion-corrected CBCT in GEJ and pancreas, RMC-CBCT yielded improved organ visibility and localization accuracy for gated treatment at end expiration in the majority of cases.

### ARTICLE HISTORY



Received 9 February 2017  
Accepted 9 January 2018

### Introduction

Modern linear accelerators use gantry-mounted cone-beam computed tomography (CBCT) for visualizing tumors and organs at risk (OAR), to correct patient position just prior to radiation treatment. Current clinical CBCT scan acquisition time is approximately 1 min for a 360° scan. Since the typical patient breathing period is 10–20 times shorter, respiratory motion during a free breathing scan is unavoidable. Image quality in CBCT of respiratory sites, in thorax and abdomen, is adversely affected by respiratory motion, as it blurs the tumor and nearby organs at risk, which makes visualization of organ boundaries difficult.

Respiration-correlated CBCT (4D-CBCT), using slow continuous gantry rotation, or multiple rotations, to produce a


series of images over the breathing cycle, has been studied by several investigators [1–3]. These references discuss degradation of imaging quality due to the reduced number of projection images and view aliasing streak artifacts caused by uneven projection spacing. For this reason, 4D-CBCT has been limited in most cases to lung where soft tissue contrast is large. Shimohigashi et al. have investigated changes in tumor motion in liver, using 4D-CBCT in combination with abdominal compression [4]. More recently, investigators have considered alternative acquisition and reconstruction methods, and reported some improvement in the image quality of 4D-CBCT [5,6]. In a prospective study of lung and abdomen scans by our group, gated CBCT (G-CBCT) at end expiration was shown to reduce image blurring and streaking artifacts

**CONTACT** Gig S. Mageras  [magerasg@mskcc.org](mailto:magerasg@mskcc.org)  Department of Medical Physics, Memorial Sloan Kettering Cancer Center, 1275 York Avenue, New York 10065, NY, USA

\*Present address: Department of Radiation Oncology, SUNY Upstate, Medical University, Syracuse, NY 13210, USA.

†Present address: Department of Radiation Oncology, University of Colorado Cancer Center, Aurora, CO 80045, USA.

‡Present address: Department of Radiation Oncology, Long Island, Jewish Medical Center, New Hyde, Park, NY 11040, USA.

 Supplemental data for this article can be accessed [here](#).

caused by respiratory motion, with mean scan duration approximately 5 min [7]. These developments notwithstanding, acquisition times and patient imaging doses were still greater than for standard one-minute free breathing CBCT scans.

Application of respiratory motion models to free breathing CBCT data can provide an alternative to the above-mentioned techniques [8]. In particular, patient-specific models derived from respiration-correlated CT (4DCT) scans on a dedicated CT scanner have been used to generate deformation vector fields to correct motion artifacts in one-minute CBCT images and produce images at individual respiratory states [9–11]. In a retrospective study, Rit et al. have reported that respiratory motion corrected CBCT (RMC-CBCT) is of particular value for tumors in lung that move more than 1 cm and provides sufficient image quality, relative to 4D-CBCT, to be clinically useful [12]. In a prospective study of lung tumors by our group, Dzyubak et al. reported reduced motion artifacts and improved tumor localization accuracy using RMC-CBCT [13].

The results mentioned have shown promise for motion correction in lung, where soft tissue contrast is large and our earlier study reported one clinical example in abdomen that demonstrated reduced motion artifacts but did not evaluate organ localization accuracy [11]. We report here on a prospective study that evaluates a respiratory motion corrected CBCT approach in upper abdominal disease sites. Our study focuses on producing a motion-corrected CBCT for guiding free-breathing gated treatment at end-expiration. We follow an approach similar to that described in our earlier study [11]. In addition to larger patient statistics, we evaluate the method's ability to reduce motion artifacts and improve soft tissue localization accuracy in one-minute CBCT scans. The latter is made possible by introducing a novel method of G-CBCT [7] as a criterion standard for comparison. To our knowledge, this is the first prospective study of motion-corrected CBCT in abdominal disease sites. Application and evaluation of this method in abdomen are more challenging than in lung, owing to the lower soft tissue contrast and organ visibility.

## Material and methods

The prospective study compared standard clinical CBCT images having no motion correction (NC-CBCT) with CBCT images (RMC-CBCT) at end expiration, both reconstructed from the same one-minute scan. A respiration G-CBCT acquired at end expiration served as the criterion standard [7].

### Patient study

Patient data for this prospective study were obtained from January 2011 through January 2014 in an Institutional Review Board (IRB) approved protocol (IRB Number 10-146) with informed consent. Eligible patients were those receiving radiation treatment of a malignancy in gastroesophageal junction (GEJ) or pancreas, that exhibited at least 5 mm motion in a 4DCT scan obtained at treatment simulation (described below). Patient data analyzed in the study

included 11 in GEJ and five in pancreas. The 16 patients included 10 females and six males. The mean age was 56.4 years (standard deviation 9.6, range 43–75). Only two patients were excluded from the analysis. One patient, in the GEJ data set, was excluded because the patient did not understand the instructions and breathed extremely erratically which made the CBCT and 4DCT images unusable. One patient, in the pancreas data set, was excluded because the patient did not have implanted fiducials and the implanted stent (in the common bile duct) was not visible in some of the binned CBCT images to permit its use as a surrogate for motion-corrected CBCT.

Patients received a helical CT scan for planning purposes and 4DCT scan (8-slice Lightspeed, GE Medical Systems, Waukesha, WI, USA) as part of their treatment simulation. The 4DCT was obtained from an axial scan in cine mode, which was acquired while recording the patient's respiration (Real-time Position Management RPM, Varian Medical Systems, Palo Alto, CA, USA). The monitoring system consisted of a block with infrared reflective markers, placed on the patient's abdomen and monitored by a stereoscopic camera. Acquisition time per couch position was set to the patient's respiration period plus 1 s, with gantry rotation period of 0.5 s. The time interval between consecutive images was the greater of either 1/20 of the respiration period or 0.25 s. Slice width was 0.25 cm. The slices were sorted into 10 phase bins (GE Advantage 4D) that comprised the 4DCT image set. The simulation 4DCT images were used for treatment planning purposes and for determining patient eligibility to enter the protocol (described below).

Patient simulation day 4DCT images were screened for excessive motion artifacts due to irregular breathing. GEJ patients allergic to oral barium contrast or pancreas patients allergic to IV iodine contrast were excluded from entering the study.

Patients underwent research scans on one day in the first week of treatment (typically two to three weeks following treatment simulation), consisting of:

1. Respiration G-CBCT prior to both the one-minute CBCT and radiation treatment, using a phase gate spanning approximately 35% of the breathing cycle, centered at end-expiration (EE) [7]. The mean acquisition time was 4.8 min (range 3.4–7.1).
2. Standard one-minute CBCT scan prior to radiation treatment, acquired in the clinical mode of operation, in which the gantry rotated continuously at approximately 6°/s while kV projection images were acquired at 11 images/s.
3. A second one-minute CBCT scan, immediately after treatment.
4. A cine CT scan on a dedicated CT scanner, either before or after the treatment session, which served to produce an amplitude-sorted 4DCT (described in the [Supplemental Material](#)).

CBCT scans were performed on a computer-controlled linac (TrueBeam, Varian Medical Systems), which had

capabilities for synchronizing motions of all mechanical axes with MV dose delivery and kV image acquisition, either with or without respiratory gating. All CBCT scans consisted of 360-degree rotation in half-fan mode (i.e., detector laterally offset 16 cm to obtain a 46 cm reconstructed diameter), with settings of 125 kV, and 11 images/s. Gated scan image settings were 80 mA and 20 ms. Clinical scan image settings were 112 mA and either 27 or 20 ms, depending on the version of treatment control software. The RPM respiratory monitoring system was used to provide an external respiratory reference, for all scans. Patients were advised to relax and breathe regularly throughout all scans. A medical physicist was always present to guide the radiation therapist through the procedures.

For the purposes of the analysis in this article, comparison of RMC-CBCT and NC-CBCT was different for each disease site: (1) In GEJ, patients received 200 cc oral contrast containing 2% barium sulfate suspension prior to the G-CBCT scan. The one-minute scan prior to treatment was used for RMC- and NC-CBCT, such that the oral contrast was visible in the gated, RMC- and NC-CBCT images. The approximate time between the gated and pretreatment one-minute scans was 9 min. (2) In pancreas, the one-minute scan after treatment was used for RMC- and NC-CBCT. Pancreatic patients received intravenous (IV) contrast prior to the pretreatment one-minute scan, for evaluating a protocol study goal not analyzed in this article. Therefore, in order to minimize the influence of residual IV contrast in comparing to the G-CBCT (without contrast) the post-treatment one-minute scan (rather than the pretreatment scan) was used in the analysis of pancreatic cases. The approximate time between the gated and post-treatment one-minute scans was 20 min. In both disease sites, the G-CBCT image acquired before treatment served as a criterion standard in the comparison.

In this study, the respiratory motion-corrected CBCT (RMC-CBCT) was based on a patient-specific motion model derived from the amplitude-sorted 4DCT acquired on the same treatment day as the CBCT scans [11]. Details of the generation of the motion model and its application to the RMC-CBCT are described in the [Supplemental Material](#). In addition, a CBCT image without motion correction (NC-CBCT) was generated (Section 'Reconstruction of uncorrected cone-beam CT' and Figure SM-1 in the [Supplemental Material](#)). The projection data, binning and reconstruction processes of the NC-CBCT and RMC-CBCT were identical except for the application of motion correction in the latter image. This was done in order to avoid confounding factors in the comparative process, arising from possible differences in X-ray scatter corrections from the reconstruction methods.

## Analysis

Analysis was performed using a treatment planning system developed at this institution [14]. Determination of the target localization discrepancy used the following procedure. First, a rigid registration was performed on the test image (NC-CBCT or RMC-CBCT) to the reference G-CBCT using the vertebral bodies, which removed any patient setup errors.

Rigid registration was first done automatically, and adjustments were done manually if needed. The automatic process adjusted test image translations and rotations relative to the reference image so as to maximize, within a volume of interest (VOI) around the object to be aligned in the two images, the normalized cross-correlation cost function (NCC) where  $g_1$  and  $g_2$  were pixel intensities, and  $\mu_1$  and  $\mu_2$  were mean pixel intensities, within the VOI of  $n$  voxels on the two images, respectively [15]:

$$\text{NCC} = \frac{\sum_{i=1}^n [(g_{1i} - \mu_1) \times (g_{2i} - \mu_2)]}{\left[ \sqrt{\sum_{i=1}^n (g_{1i} - \mu_1)^2} \times \sqrt{\sum_{i=1}^n (g_{2i} - \mu_2)^2} \right]} \quad (1)$$

An NCC of one indicated perfect congruence between the two images. The presence of image artifacts such as streaks could also affect the NCC value.

Next, a second manual rigid registration was performed, without allowing rotations, using soft tissue features when possible and fiducials if necessary, to align near the GEJ (for GEJ patients), or GTV (for pancreas patients). For pancreas patients, the second registration was also performed for each kidney. The localization discrepancy was computed as the 3D difference in translation between the vertebral body registration and the secondary registration. To determine the reproducibility of the match procedure, the secondary registration was performed by the same observer on three separate days.

A possible contribution to localization discrepancy was that the target in the G-CBCT may not be in the same position as in the one-minute CBCT owing to changes in breathing pattern. To estimate this contribution, we measured the discrepancy in the position of fiducials relative to the skeletal anatomy (of patients with implanted fiducials), between the G-CBCT and a CBCT image generated by selecting those binned CBCT images from the one-minute scan around end expiration, consistent with the gate interval used in the G-CBCT. That is, for a given RPM start and end phase for the gate (typically 30 and 70%) the corresponding amplitude-binned CBCT images (typically 30–70th amplitude percentiles, as described in the [Supplemental Material](#)) were chosen. The selected images were averaged but uncorrected for motion and the resultant image was rigidly registered twice to the G-CBCT, first to align the vertebral columns and second to align the fiducials. The difference in translations between the two registrations was an estimate of the change in target position between the two scans.

In the GEJ patient cases, the esophagus and stomach contours delineated by the physician on the planning CT were used as a guide to delineate the GEJ on the G-CBCT image (the GE junction itself was not delineated on the planning CT). A 5 mm 2D annulus was constructed around the GEJ to serve as a region of interest (ROI) for quantitative assessment of image similarity. These contours were delineated by a physicist and approved by a physician. In the pancreas cases, the kidneys were delineated by a trained physicist on the G-CBCT image. A 5 mm 3D annulus around each kidney served as an ROI.

Similarity in object size and shape within each ROI was measured, between the NC- and G-CBCT and between the RMC- and G-CBCT, after each secondary alignment (described above), by calculating the NCC.

## Results

### Patient studies in gastroesophageal junction

Figure 1 shows an example of CBCT images with and without motion correction, in the vicinity of the GE junction. The GEJ tumor in this example exhibited 6.5 mm motion extent in the 4DCT acquired on the same day as the CBCT scans. The NC-CBCT showed more motion-induced streak artifacts in the transaxial image and more motion blurring in the coronal image than RMC-CBCT. The motion artifacts and blurring in the NC-CBCT severely limited the visibility of the GEJ, whereas the visibility of the GEJ in the RMC-CBCT was comparable to that in the G-CBCT.

Comparison of GEJ localization discrepancy (Figure 2) showed smaller mean discrepancy in the RMC-CBCT relative to NC-CBCT in eight of eleven patients. A paired two-tailed *t*-test showed statistical significance ( $p = .03$ ). The patient mean  $\pm$  standard deviation discrepancy for NC-CBCT and RMC-CBCT was  $0.43 \pm 0.28$  and  $0.21 \pm 0.11$  cm, respectively. The uncertainty in the mean localization discrepancy (error bars in the plot) was larger in the NC-CBCT data in nine of eleven cases, but was not statistically significant ( $p = .2$ ). This reflected the larger variability in the NC-CBCT to G-CBCT registration, owing to the larger amount of blurring and streaking artifacts that obscured the GE junction in the NC-CBCT.

Analysis of discrepancy in fiducial positions between the gated and one-minute CBCT scans in GEJ patients (owing to changes in breathing pattern between the two scans), yielded a mean  $\pm$  standard deviation 3D distance of  $0.28 \pm 0.25$  cm.

Figure 3 compares the NCC, relative to the G-CBCT, of soft tissue features in the vicinity of the GEJ. The RMC-CBCT yielded higher NCC than NC-CBCT in nine of eleven

patients ( $p = .03$ ). This indicated higher congruence with the criterion-standard G-CBCT for RMC-CBCT than NC-CBCT. Patient mean  $\pm$  standard deviation GEJ NCC for NC-CBCT and RMC-CBCT was  $0.43 \pm 0.21$  and  $0.48 \pm 0.20$ , respectively.

### Patient studies in pancreas

Figure 4 shows an example of CBCT images with and without motion correction in the vicinity of the pancreas. The NC-CBCT showed more motion-induced streak artifacts in the transaxial image and more motion blurring in the sagittal image than RMC-CBCT. The RMC-CBCT image increased the visibility of the pancreas; in addition, there was a clear reduction in the blurring of the fiducial. Some streak artifacts in the transaxial images were caused by motion of gas in the stomach and bowel during the CBCT scan, which was not

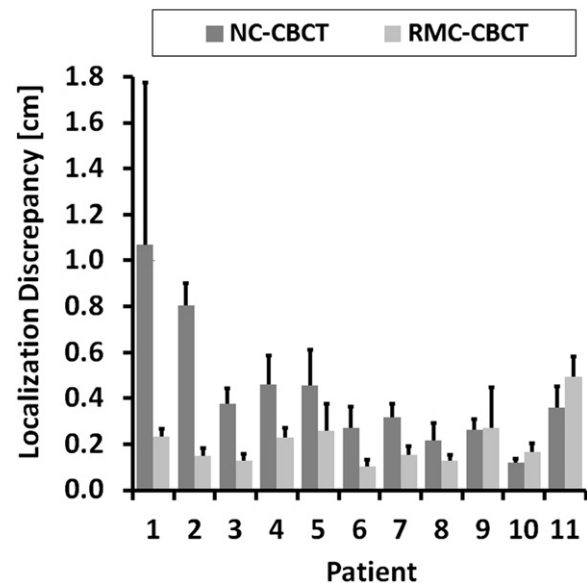


Figure 2. Gastroesophageal junction mean (across repeat measurements) 3D localization discrepancy for eleven patients, in order of decreasing difference between no-correction NC-CBCT and RMC-CBCT. Error bars are standard error of the mean, only upper error bars are shown.

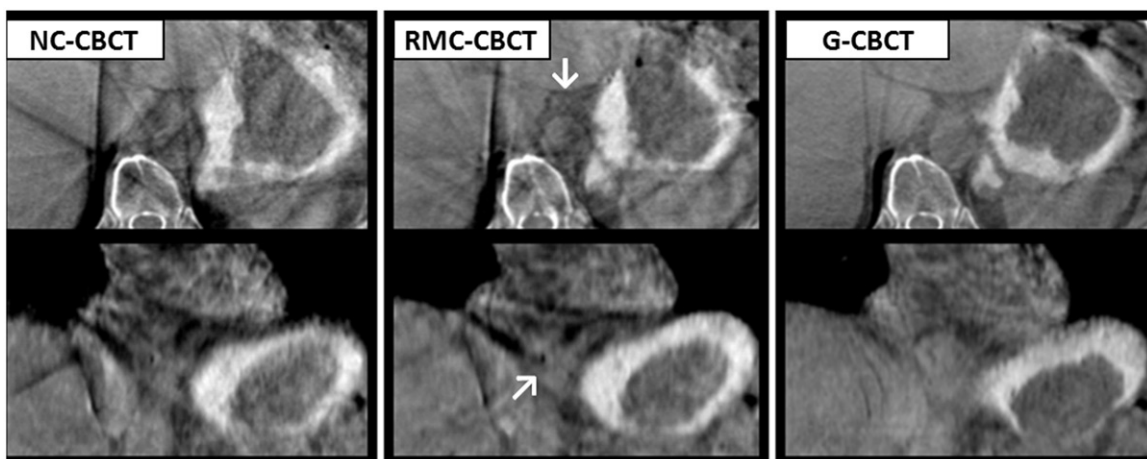
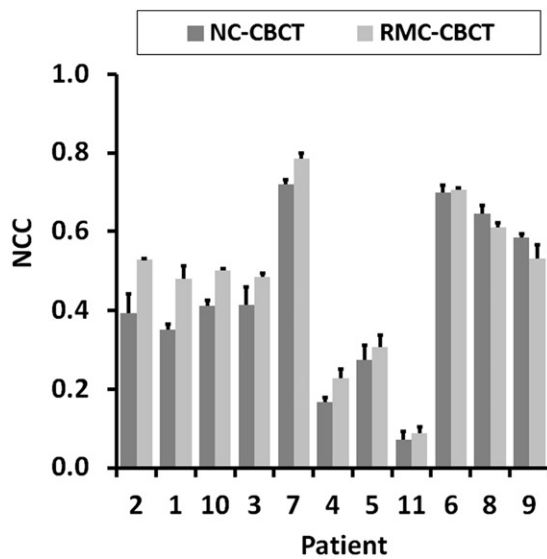


Figure 1. Transaxial (top row) and coronal (bottom) CBCT images of a patient with malignancy in gastroesophageal junction (GEJ). Image planes intersect in the GEJ. Left column is NC-CBCT, middle is RMC-CBCT and right is G-CBCT. Arrows indicate soft tissue features near the GEJ in the RMC-CBCT. Barium contrast in the stomach is visible in all images. The same window/level display settings are used for all images.



**Figure 3.** Gastroesophageal junction normalized cross-correlation (NCC) for eleven patients, in order of decreasing improvement in NCC between RMC-CBCT and NC-CBCT.

corrected by our method. Streak artifacts were also visible in the G-CBCT image.

Comparison of GTV localization discrepancy (Figure 5) showed RMC-CBCT to have reduced mean discrepancy relative to NC-CBCT in all five patients ( $p = .05$ ). Patient mean  $\pm$  standard deviation discrepancy for NC-CBCT and RMC-CBCT was  $0.42 \pm 0.29$  and  $0.26 \pm 0.21$  cm, respectively.

Analysis of discrepancy in fiducial positions between the gated and one-minute CBCT scans yielded a mean  $\pm$  standard deviation 3D distance of  $0.35 \pm 0.18$  cm. Patient 2 in Figure 5 exhibited a large (0.66 cm) discrepancy in fiducial position, which may have contributed to the relatively large GTV localization discrepancy observed in both the NC-CBCT and RMC-CBCT (0.9 and 0.6 cm, respectively).

Comparison of the kidney localization discrepancy (Figure SM-2 in the Supplemental Material) showed the RMC-CBCT to have reduced mean discrepancy relative to NC-CBCT for all 10 kidneys ( $p = .002$ ). The uncertainty in mean discrepancy (error bars in the plot) was larger in the NC-CBCT data for eight of ten kidneys ( $p = .04$ ). Patient mean  $\pm$  standard

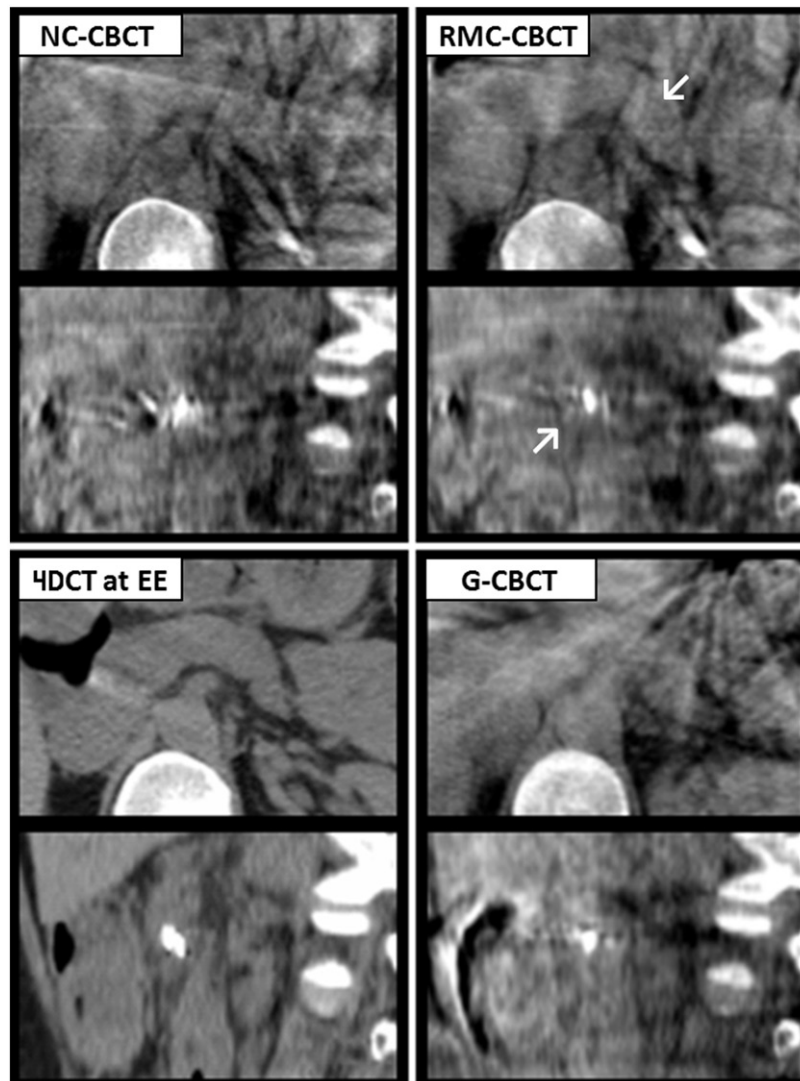


**Figure 4.** Transaxial and sagittal CBCT images of a free breathing patient treated for pancreatic cancer. Image planes intersect in the pancreas, superior to the fiducial. Upper left panel is no-correction NC-CBCT, upper right is RMC-CBCT, lower right is G-CBCT and lower left is 4DCT at end expiration. Arrows indicate pancreas in the RMC-CBCT. The residual IV contrast, administered after the G-CBCT and prior to treatment, caused the post-treatment NC-CBCT and RMC-CBCT images to appear brighter than the G-CBCT and 4DCT. The same window/level settings were used for all images.

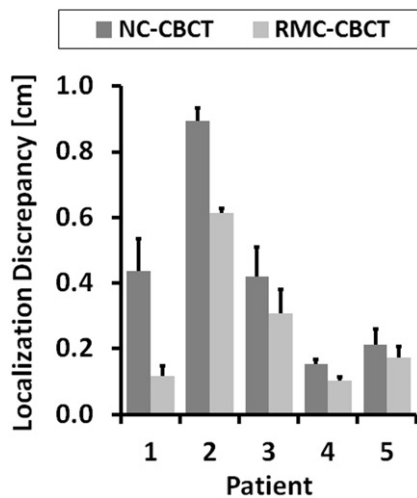


**Figure 5.** GTV region mean 3D localization discrepancy for five pancreatic cancer patients, in order of decreasing difference between NC-CBCT and RMC-CBCT.

deviation discrepancy for NC-CBCT and RMC-CBCT was  $0.51 \pm 0.25$  and  $0.19 \pm 0.13$  cm, respectively.

Analysis of similarity in soft-tissue features (Figure SM-3 in the [Supplemental Material](#)) showed that RMC-CBCT yielded higher NCC than NC-CBCT in eight of ten kidneys ( $p = .01$ ). This indicated higher congruence between the motion-corrected and G-CBCT. Patient mean  $\pm$  standard deviation kidney NCC for NC-CBCT and RMC-CBCT was  $0.40 \pm 0.17$  and  $0.44 \pm 0.16$  cm, respectively.

## Discussion

In a prospective study of 16 abdominal cancer patients (eleven GEJ and five pancreas), we have evaluated the efficacy of RMC-CBCT to reduce motion artifacts and improve end-expiration localization accuracy. To our knowledge, this is the first prospective study of motion-corrected CBCT in abdominal sites. The study examined end expiration as the motion-corrected state, which allowed comparison to a G-CBCT technique, also acquired at end expiration, as a criterion standard. Although gated CBCT also yielded images with reduced motion artifacts and improved localization accuracy, a limitation was the longer acquisition times, which in an earlier study averaged approximately, 5 min (range 3–8 min) [7]. The focus of this study was to assess the suitability of motion-corrected CBCT for guiding gated treatment at end expiration, which is used at our institution [16]. The method could also be applied to a mid-ventilation or respiratory-averaged position but this was not addressed in this study. Our findings indicated that RMC-CBCT reduced motion artifacts, improved organ visibility and reduced localization error for end-expiration gated treatment in the majority of abdominal images.

Our finding, that tumor location in the RMC-CBCT was in better agreement with the gated G-CBCT than the uncorrected NC-CBCT, was in accordance with expectations, since RMC-CBCT was intended to depict end expiration whereas NC-CBCT depicted a respiration-averaged image. The rationale of this experiment was to assess to what extent

RMC-CBCT improved upon the current standard of care (i.e., NC-CBCT) in the context of localization for gated treatment at end expiration. A possible further experiment, not investigated in this study, is to compare end-expiration localization by RMC-CBCT with localization by NC-CBCT that is corrected for the motion between end-expiration and respiration-averaged positions, for example, as obtained from the 4DCT at simulation. The latter approach does not account for variations in breathing amplitude between simulation and treatment.

The localization discrepancy observed between RMC-CBCT and G-CBCT differed between the two patient groups. Localization discrepancy of GEJ was  $0.21 \pm 0.11$  cm (range 0.1–0.5 cm), which was consistent with changes in fiducial position ( $0.28 \pm 0.25$  cm) between the gated and one-minute CBCT scans. In the pancreatic group, however, there was larger localization discrepancy of the GTV ( $0.26 \pm 0.21$  cm; range 0.1–0.6 cm) and larger changes in fiducial position ( $0.35 \pm 0.18$  cm). The differences between the two groups may have been a consequence of the different elapsed time between gated and one-minute CBCT scans: in the GEJ group, both scans were acquired before treatment and were approximately 9 min apart, whereas in the pancreatic group, the post-treatment one-minute CBCT scan was analyzed for this study (as explained in the Material and Methods Section), which was approximately 20 min after the G-CBCT. The longer elapsed time between the two scans may have increased the likelihood of respiration-induced baseline drift in some patients. For the purpose of determining the improvement in localization accuracy with RMC-CBCT, our protocol was designed to acquire all CBCT scans at the same treatment session, including the G-CBCT which served as the criterion standard. This was done in order to minimize any confounding effects of interfraction organ movement, interfraction changes in patient breathing and different patient setups.

The motion-corrected CBCT images were derived from a patient-specific motion model [17]. The model related the organ deformations in the 4DCT images to the displacement of a surrogate from its end-expiration position in the 4DCT, and its direction of motion (inspiration or expiration). As such, the motion model was not dependent on repeatable breathing cycles, and thus could be used to correct one-minute CBCT scans acquired at different times. In the study reported here, the motion correction model was obtained from a 4DCT scan acquired on the same day as the CBCT. Since the clinical process commonly acquires 4DCT at simulation, a consideration is whether the patient tumor-motion pattern may change between simulation and treatment, specifically, the relation between surrogate displacements and deformation fields. We expect this relationship to change slowly over the treatment course, thus requiring only one or two 4DCT scans, i.e., similar to adaptive planning. In a study of tumors in lung, Dzyubak et al. found that motion correction at end expiration using a 4DCT acquired at simulation yielded similar results to those using a 4DCT on the treatment day, two to three weeks after simulation [13]. Further studies are needed to examine whether these findings are applicable to motion-corrected CBCT in abdominal sites.

Other publications [10–13] have pointed out that motion-corrected CBCT, using a model derived from 4DCT, could provide useful improvement to uncorrected CBCT, and had the advantage of shorter acquisition times relative to 4D-CBCT. These studies were either retrospective, studied small numbers of patients, or were limited primarily to investigations of tumors in lung. Rit et al. reported that respiratory motion-corrected CBCT images provided good localization accuracy of lung tumors, using 4D-CBCT as a standard for comparison [12]. The image quality of 4D-CBCT suffers from view-aliasing artifacts, which limits its utility as a criterion standard. In this study, we used G-CBCT which yields a high-quality CBCT and allows a more reliable measure of localization error [7].

For clinical application to correction of patient setup, motion-corrected CBCT can be reconstructed at a respiration state that is relevant to treatment. A consistent patient geometry and motion state is desirable for both imaging and treatment. In this study, RMC-CBCT images were reconstructed at end expiration, which would be suitable to gated treatment at end expiration. For patient setup in this context, the reference image would be the simulation 4DCT at near end expiration. Any patient setup errors can be removed from the motion correction process by first applying rigid registration to align the bony anatomy (vertebral column) of the CBCT (reconstructed with all projections and before motion correction) to that in the reference 4DCT image. The translations so obtained can be then applied to the binned CBCT reconstructions, before continuing with the motion correction process.

Our finding, that localization discrepancy at end expiration between RMC-CBCT and G-CBCT is reduced compared to uncorrected CBCT, supports the application of RMC-CBCT to gated treatment. Integration into the clinical process for evaluating patient setup is feasible by means of automatic localization of implanted fiducial markers in the projection images during the CBCT scan [18]. The detected fiducial trajectory would serve to bin the projections for CBCT reconstruction and as the surrogate for application of the motion model to deform each binned CBCT to the reference state.

For clinical implementation, computational processing time must be minimized. The current processing time is approximately 5 min, for amplitude sorting, reconstruction and motion correction, on an Intel Xeon E5-2620 2 GHz dual-processor workstation. This could be substantially improved by introducing more processors or GPU programming.

There are several limitations of our study. One is that the motion correction process can be hindered by streaking due to implanted stents and by inconsistent patient breathing. Two cases (mentioned in the Material and Methods Section) were excluded for these reasons. Another limitation is the manual determination of internal surrogate positions in the 4DCT and binned CBCT images. In cases where implanted fiducials exist, their position can be automatically detected in the CBCT projection images [18]; we have recently implemented such capability for motion-corrected CBCT immediately prior to treatment. Determination of fiducial positions in the 4DCT image set can be accomplished by propagation

of contours following deformable image registration between the reference image and other images in the 4DCT set [19], but this was not attempted in this study.

Another of our study goals was to investigate the improvement in image quality and soft tissue visibility with the proposed method. Our method of reconstructing the uncorrected CBCT was chosen so as to avoid confounding factors when comparing corrected and uncorrected image quality, arising from differences in x-ray scatter corrections between our method of reconstruction (sum of 10 binned reconstructions) and a single reconstruction using all projections. The resultant images from the two reconstruction approaches yield small variations in image shading and negligibly small differences in organ positions and shapes (details are in the Section ‘Reconstruction of uncorrected cone-beam CT’ in the [Supplemental Material](#)).

In addition to respiration-induced motion, CBCT in the abdomen is also subject to artifacts from bowel and stomach motion. Nevertheless, respiratory management such as breath hold yields CBCT image quality in abdomen that is clinically useable for image-guided treatment [20]. Our previous study showed that the visibility of soft tissue organs in abdomen is improved with G-CBCT [7]. At present, our institution routinely uses breath-hold CBCT without contrast for image-guided ablative radiotherapy of liver tumors and pancreatic cancer. Cone-beam CT is important when the tumor is near the gastrointestinal tract, even when implanted fiducial markers are present [21]. In this context, adaptive planning is triggered when stomach and/or small bowel positions as observed in cone-beam CT at treatment are consistently different from those in the simulation CT [22].

In summary, in a prospective clinical study of motion-corrected CBCT in GEJ and pancreas, RMC-CBCT was found to improve organ visibility and localization accuracy for gated treatment at end expiration in the majority of abdominal images.

## Disclosure statement

No potential conflict of interest was reported by the authors.

## Funding

The work was supported in part by the United States National Cancer Institute [grant numbers R01 CA126933 and P30 CA008748] and a research agreement with Varian Medical Systems.

## References

- [1] Sonke JJ, Zijp L, Remeijer P, et al. Respiratory correlated cone beam CT. *Med Phys*. 2005; 32:1176–1186.
- [2] Lu J, Guerrero TM, Munro P, et al. Four-dimensional cone beam CT with adaptive gantry rotation and adaptive data sampling. *Med Phys*. 2007;34:3520–3529.
- [3] Bergner F, Berkus T, Oelhafen M, et al. An investigation of 4D cone-beam CT algorithms for slowly rotating scanners. *Med Phys*. 2010;37:5044–5053.
- [4] Shimohigashi Y, Toya R, Saito T, et al. Tumor motion changes in stereotactic body radiotherapy for liver tumors: an evaluation

- based on four-dimensional cone-beam computed tomography and fiducial markers. *Radiat Oncol.* 2017;12:61–68.
- [5] Jia X, Tian Z, Lou Y, et al. Four-dimensional cone beam CT reconstruction and enhancement using a temporal nonlocal means method. *Med Phys.* 2012;39:5592–5602.
- [6] Shieh CC, Kipritidis J, O'Brien RT, et al. Image quality in thoracic 4D cone-beam CT: a sensitivity analysis of respiratory signal, binning method, reconstruction algorithm, and projection angular spacing. *Med Phys.* 2014;41:041912.
- [7] Kincaid RE, Yorke ED, Goodman KA, et al. Investigation of gated cone-beam CT to reduce respiratory motion blurring. *Med Phys.* 2013;40:041717.
- [8] McClelland JR, Hawkes DJ, Schaeffter T, et al. Respiratory motion models: a review. *Med Image Anal.* 2013;17:19–42.
- [9] Brehm M, Paysan P, Oelhafen M, et al. Artifact-resistant motion estimation with a patient-specific artifact model for motion-compensated cone-beam CT. *Med Phys.* 2013;40:101913.
- [10] Rit S, Wolthaus JWH, van Herk M, et al. On-the-fly motion-compensated cone-beam CT using an a priori model of the respiratory motion. *Med Phys.* 2009;36:2283–2296.
- [11] Zhang Q, Hu YC, Liu F, et al. Correction of motion artifacts in cone-beam CT using a patient-specific respiratory motion model. *Med Phys.* 2010;37:2901–2909.
- [12] Rit S, Nijkamp J, van Herk M, et al. Comparative study of respiratory motion correction techniques in cone-beam computed tomography. *Radiother Oncol.* 2011;100:356–359.
- [13] Dzyubak O, Kincaid R, Hertanto A, et al. Evaluation of tumor localization in respiration motion-corrected cone-beam CT: prospective study in lung. *Med Phys.* 2014;41:101918 (10 pp).
- [14] Mageras GS, Hu YC, McNamara S, et al. Imaging for radiation treatment planning. In: Starkschall G, Siochi RAC, editors. *Informatics in radiation oncology.* Boca Raton (FL): CRC Press; 2013. p. 15.
- [15] Gonzales RC, Woods RE. *Digital image processing.* Reading (MA): Addison-Wesley; 1992. p. 584.
- [16] Liu F, Ng S, Huguet F, et al. Are fiducial markers useful surrogates when using respiratory gating to reduce motion of gastroesophageal junction tumors? *Acta Oncol.* 2016;55:1040–1046.
- [17] Zhang Q, Pevsner A, Hertanto A, et al. A patient-specific respiratory model of anatomical motion for radiation treatment planning. *Med Phys.* 2007;34:4772–4781.
- [18] Regmi R, Lovelock DM, Hunt M, et al. Automatic tracking of arbitrarily shaped implanted markers in kilovoltage projection images: a feasibility study. *Med Phys.* 2014;41:071906.
- [19] Starkschall G, Britton K, McAleer MF, et al. Potential dosimetric benefits of four-dimensional radiation treatment planning. *Int J Radiat Oncol Biol Phys.* 2009;73:1560–1565.
- [20] Hawkins MA, Brock KK, Eccles C, et al. Assessment of residual error in liver position using kV cone-beam computed tomography for liver cancer in high-precision radiation therapy. *Int J Radiat Oncol Biol Phys.* 2006;66:610–619.
- [21] Crane CH, Koay EJ. Solutions that enable ablative radiotherapy for large liver tumors: fractionated dose painting, simultaneous integrated protection, motion management, and computed tomography image guidance. *Cancer.* 2016;122:1974–1986.
- [22] Crane CH. Hypofractionated ablative radiotherapy for locally advanced pancreatic cancer. *J Radiat Res.* 2016;57:i53–i57.